Appl. Phys. B 83, 235–239 (2006)
DOI: 10.1007/s00340-006-2171-8

Applied Physics B
Lasers and Optics

J.E. HELLSTRÖM[1,✉]
S. BJURSHAGEN[1]
V. PASISKEVICIUS[1]
J. LIU[2]
V. PETROV[2]
U. GRIEBNER[2]

Efficient Yb:KGW lasers end-pumped by high-power diode bars

[1] Department of Physics, Royal Institute of Technology, Stockholm 10044, Sweden
[2] Max-Born Institute, Max-Born Strasse 2A, 12489 Berlin, Germany

Received: 15 December 2005 /
Revised version: 8 February 2006
Published online: 29 March 2006 •

ABSTRACT The laser performance of Yb:KGW under end-pumping with high-power diode bars has been investigated. In one configuration, the pump is delivered through an optical fiber yielding a symmetric but unpolarized pump spot. In the second configuration, the pump is delivered through an optical lens system yielding a polarized but asymmetric pump spot. Both configurations resulted in a maximum optical to optical efficiency of 47% and a maximum power of 12.4 W has been generated with the fiber coupled pump source. The output power was limited by crystal fracture, which occurred at an estimated temperature gradient of 1.2×10^5 K/m. Thermal lensing and laser tuning characteristics are also investigated.

PACS 42.55.Xi; 42.60.Lh

1 Introduction

Recently, increased interest has been shown in Yb^{3+}-doped double tungstates such as Yb:$KGd(WO_4)_2$ (Yb:KGW), Yb:$KY(WO_4)_2$ (Yb:KYW) an Yb:$KLu(WO_4)_2$ (Yb:KLuW) as the laser material with the highest potential for efficient tunable continuous wave (cw) and mode-locked operation in diode-pumped arrangements. The advantageous features of these materials are high absorption and emission cross sections, as well as acceptance of high doping concentrations without indication of serious quenching [1–3]. Low quantum defect and absence of parasitic effects such as upconversion or excited state absorption have enabled demonstration of high cw slope efficiencies in both, Ti:Sapphire and laser diode-pumped setups [1–9]. The possibility of a large doping concentration is also beneficial for thin-disk laser designs which have been demonstrated in cw [2, 6, 8], the mode-locked regime [10] as well as in high-average power femtosecond regenerative amplifier [11]. The thin-disk configurations alleviate to a large degree the problems associated with thermal loading and relatively poor thermal conductivity in double tungstates. For instance, the thermal conductivity in KYW of 3.3 $Wm^{-1}K^{-1}$ is about three-times lower than in YAG or Lu_2O_3 [2].

✉ Fax: +46-8-5537 8216, E-mail: jh@laserphysics.kth.se

End-pumping schemes, however, offer in most cases more compact and less expensive laser designs, where the matching of the laser mode and the pump beam can be achieved relatively easy. This is an important issue considering the three-level nature and corresponding reabsorption in Yb^{3+} transitions around 1 μm. The highest slope efficiencies have been reported for end-pumped configurations [1, 4, 7, 9]. End-pumped configurations are also more favorable for compact lasers or Q-switched lasers with short pulse lengths than the multi-pass thin disc configurations. Recent analysis by Brenier et al. [12, 13] reveals that KYW and KGW (at that time KLuW was still not introduced) should be the most promising Yb^{3+} hosts for end-pumped cw lasers. This conclusion stems primarily from the calculations of the laser output yield (or optical efficiency) $\frac{P_{\text{out}}}{P_{\text{pump}}}$ and slope efficiency $\frac{\mathrm{d}P_{\text{out}}}{\mathrm{d}P_{\text{pump}}}$, which are more relevant than sometimes used figures of merit such as gain cross section and minimum pump intensity required for achieving transparency, $I_{\min} = \frac{\sigma_a h\nu}{(\sigma_{ap}\tau(\sigma_a+\sigma_e))}$ [14]. Here, σ_a, σ_e are the absorption and emission cross sections at the laser wavelength, σ_{ap} is the absorption cross section of pump, τ is the lifetime of the $^2F_{5/2}$ level and $h\nu$ is the laser photon energy.

The most efficient end-pumped laser configuration reported appears to be pumping by a gain-switched Ti:sapphire laser [4]. In this set-up the slope efficiency with respect to the absorbed power reached 86% and the output yield was around 50%. Under diode pumping, the most efficient configurations have used Yb:KLuW pumped by a fiber-coupled diode focused to a spot of ∼ 40 μm [7]. Here the slope efficiencies with respect to the incident pump power reached 78% (87% with respect to the absorbed power) and the optical efficiency was around 50%. In these demonstrations relatively low power and high-brightness pump sources have been used and the maximum generated power did not exceed 3.5 W.

In this work we aim at extending the generated power in the end-pumped Yb:KGW laser arrangements using diode bar pumping. The pump spot size in this case is necessarily larger than in single-emitter diode pump sources. Moreover, considering a strong asymmetry of the absorption cross section, thermal expansion and thermooptic coefficients in KGW [15], it is important to investigate different pumping configurations. Here we compare two different pumping schemes. In the first scheme, the pump is delivered through an optical fiber yield-

ing a symmetric but unpolarized pump spot. In the second scheme the pump is delivered through an optical lens system yielding a polarized but asymmetric pump spot.

2 Experimental set-up

Throughout this work a 5% Yb:KGW laser crystal was utilized. The dimensions of the laser crystal were $3 \times 3 \times 3\,\mathrm{mm}^3$, and it was cut for propagation along the optical axis N_p that is parallel with the crystallographic axis b. Both end facets of the crystal were AR-coated. The laser crystal was wrapped in an In-foil and pressed into a copper holder that was water-cooled by a temperature-controlled chiller. The input coupler consisted of a flat, dichroic mirror which was coated for high reflectivity in the 1020–1100 nm range and high transmission in the 810–980 nm range. The cavity was completed by a concave output coupler with 50 mm radius of curvature. The cavity length was adjusted for each pump source to give the highest output powers at maximum pump power.

In the first pumping scheme, the pump laser was a fiber-coupled cw diode-bar. Even though the diode holder was temperature-controlled, the pump wavelength varied between 973 nm and 980 nm by increasing the power level, resulting in an absorption under non-lasing conditions that varied between 40% and 60%. The linewidth of the laser was 4–5 nm. The maximum output power of the pump laser was 50 W at the end of the 200 μm fiber (N.A. = 0.22). The fiber output was imaged 1:1 in the center of the laser crystal, which gave a pump focus with a confocal parameter of 0.9 mm. In the second pumping scheme, we used a cw diode bar without fiber coupling as a pump source. This diode bar from LIMO GmbH was 95% linearly polarized in the direction parallel to the N_m refractive index axis. The output wavelength varied between 978–980 nm depending on power level, with a FWHM of ~ 2.5 nm. This resulted in absorption varying between 80% and 85% under non-lasing conditions. The higher absorption of the polarized diode output is easily understandable considering that the absorption cross sections for the light polarized along the N_m and N_g axes differ by as much as 8 times. The laser diode consisted of 19 individual emitters that were stacked together by use of a lens system to form a focus of 100×75 μm (e^{-2} radius) width inside the cavity. The intensity distribution of the pump was approximately Gaussian along the 75 μm dimension and closer to a top-hat along the 100 μm dimension. The confocal parameters were 1.3 mm and 5.2 mm, respectively. The maximum output power incident on the microchip after the focusing system was 19.3 W.

3 Results and discussion

The dependences of the laser output power versus the incident pump power for the two pumping schemes using different output couplers are given in Figs. 1 and 2. Here we prefer to use the incident power instead of absorbed pump power for comparison of two lasers, because of the following reasons: (a) the input power is the parameter which eventually determines the optical efficiency and matters most in practical systems, (b) the absorption saturation behavior under lasing conditions is different for the polarized and unpolarized pump: for the polarized pump the absorbed fraction

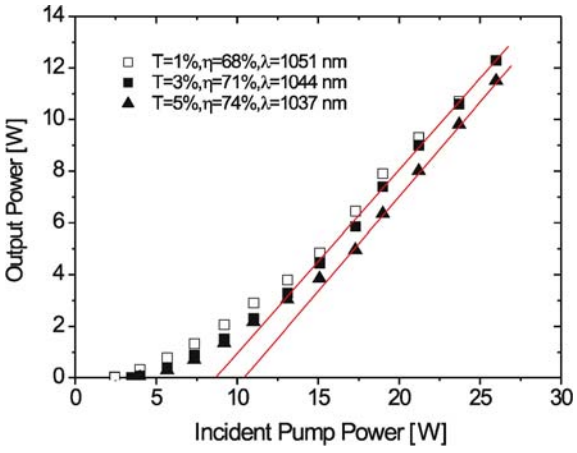

FIGURE 1 Output power versus incident power for the fiber-coupled pump for different output couplers

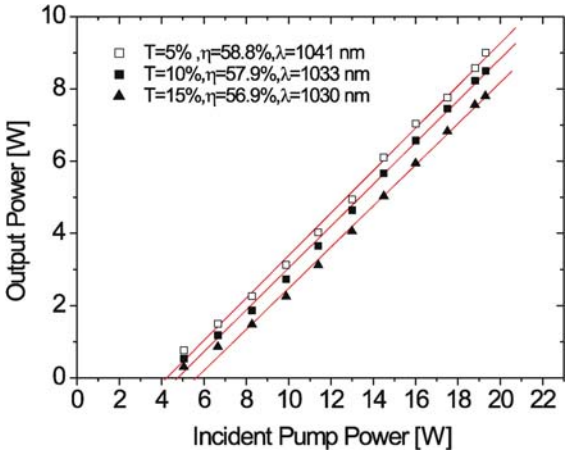

FIGURE 2 Output power versus incident power for the non-fiber-coupled pump for different output couplers

of pump power increased by about 10%–15% to reach 95% under lasing conditions. This pump recycling effect caused by the increased rate of stimulated emission should be expected in a three-level system. This effect was not so pronounced on the total absorbed power in the laser pumped with the non-polarized fiber-coupled diode due to much smaller cross sections in the N_g direction. It should also be mentioned that the use of incident pump power reduces the apparent slope efficiencies at high pump intensities. The laser threshold can be estimated from the equation [16]:

$$P_\mathrm{th} = \frac{\pi(w_\mathrm{p}^2 + w_\mathrm{c}^2)h\nu_\mathrm{p}}{4\sigma_\mathrm{e}\tau}(T + L + 2(1 - \exp(-\sigma_\mathrm{a} N_\mathrm{l} l))), \qquad (1)$$

where w_p, w_c are the pump and cavity mode radii, respectively, $h\nu$ is the pump photon energy, σ_a, σ_e are the stimulated emission and absorption cross sections at the laser wavelength, respectively. T is the output coupling, L represents the parasitic round-trip losses, N_l is the ground state population at threshold and l is the length of the laser crystal. For the beam radii of 100 μm and the emission peak wavelength of 1025 nm, cross-sections $\sigma_\mathrm{a} = 0.25 \times 10^{-20}\,\mathrm{cm}^2$, $\sigma_\mathrm{e} = 2.7 \times 10^{-20}\,\mathrm{cm}^2$ [4], $\tau = 250$ μs [17], $N_\mathrm{l} = 2.2 \times 10^{20}\,\mathrm{cm}^{-3}$, $L = 1\%$ and output coupling of $T = 5\%$. Equation (1) gives

the threshold at the absorbed pumped power of 1.8 W, an estimate which reasonably corresponds to the experimentally observed result.

The laser output characteristics in Figs. 1 and 2 are clearly nonlinear at lower pump powers as expected in the three-level system. Moreover, the nonlinearity is more pronounced in the laser pumped with the fiber-coupled laser diode, probably due to a larger variation of the diode central wavelength at higher diode currents. This leads to an increased absorption and increasing slope of the output characteristics. For the polarized pump this nonlinearity is not so pronounced primarily due to quite pronounced absorption saturation. The thresholds are generally higher for the polarized pump due to higher output coupling. However, for the $T = 5\%$ output coupler, which was tried in both set-ups, the threshold is lower for the polarized pump. The slope efficiencies with respect to the incident pump power were determined by the linear fit at the highest pump powers. In both pump configurations the highest slope efficiency was obtained using the $T = 5\%$ output coupler. So, for the polarized diode pumping the slope was about 59% while in the fiber coupled diode case the slope was as high as 74%. The higher slope in the latter case is mostly an apparent effect due to the increased absorption at higher pump powers. The maximum powers generated with the non-fiber coupled diode bar reached 9 W and was limited by the available pump power, while for the fiber coupled pumping case a maximum output power of 12.4 W was generated. By increasing the pump power further, the laser crystal fractured. This fracture occurred with 1% output coupling, resulting in a quantum defect of 7%. The generated heat was thus ~ 1.1 W and by assuming uniform pump absorption along the optical axis, the central temperature can be estimated by solving the heat transfer equation using the finite element method to 50 degrees above room-temperature. Similarly, the temperature gradient can be estimated to 1.2×10^5 K/m. For further power scaling, a more homogeneous heat distribution is required, which can be achieved, for instance, in a thin-disk laser design.

Due to the essentially nonlinear character of the laser output characteristics, the optical efficiency, i.e., the fraction of the total incident pump power converted to the laser output radiation is a more relevant performance parameter in practical devices pumped with high-power laser diodes. The dependences of the optical efficiency on the incident pump power for the laser configurations tested in this work are shown in Fig. 3. The optical efficiency is higher using the polarized non-fiber-coupled pump throughout the entire pump power interval. At the maximum incident power of 19.3 W, the optical efficiency of the non-fiber-coupled pump scheme is 47% using the $T = 5\%$ output coupler. With the same output coupler, the optical efficiency at 19.3 W of incident power is only 34% using the nonpolarized fiber-coupled pump scheme. With the lower reflectivity output couplers the optical efficiency of the fiber-coupled pump scheme is increased to 39% at 19.3 W and finally 47% at 26 W of incident pump power.

In the design of high-power diode end-pumped laser cavities, it is critical to take into account thermal lensing properties of the laser crystal. For Yb:KGW and similar hosts, a marked increase in the thermal lens power under lasing conditions has to be taken into account. It can be explained by the

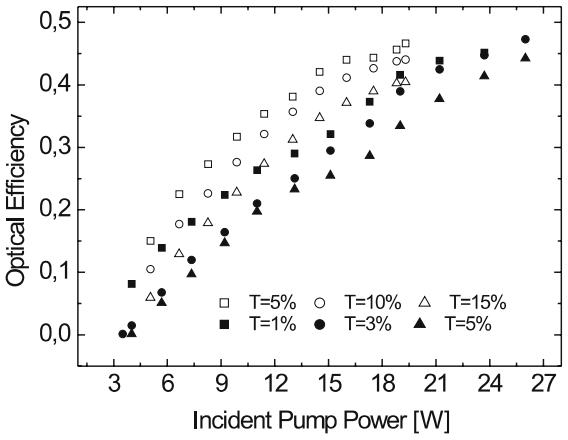

FIGURE 3 Optical efficiency versus incident power for the non-fiber-coupled pump (*empty symbols*) and the fiber-coupled pump (*filled symbols*) for different output couplers

fact that the laser operation wavelength is longer then the central fluorescence wavelength of 993 nm in Yb:KGW, which results in an increase in the thermal loading when the laser cavity is aligned. Also, an additional thermal load would be generated by the increased pump absorption in the lasing conditions. We measured the thermal lens in the crystal under lasing conditions by measuring the near and far-field distributions of a TEM_{00} beam at 532 nm wavelength and generated by a separate laser. This beam was focused into the same beam spot radius as the pump diode inside the Yb:KGW crystal. The thermal lens in Yb:KGW is astigmatic mainly due to the asymmetry in the thermal expansion in the KGW host [18]. The direction of the strongest thermal lens is rotated by about 32° from the principal optical axis N_m and is close to the X_1' principal axis of thermal expansion [19]. The focal distance of the thermal lens along this direction as a function of absorbed pump power under lasing conditions is shown in Fig. 4. The radius of curvature of 50 mm of the output coupler used in the laser cavities in this work allows the optimization of the cavity mode overlap with the pump in the plane of the stronger thermal lens. In the other direction, however, the overlap remains non-optimized, which reduces the optical efficiency.

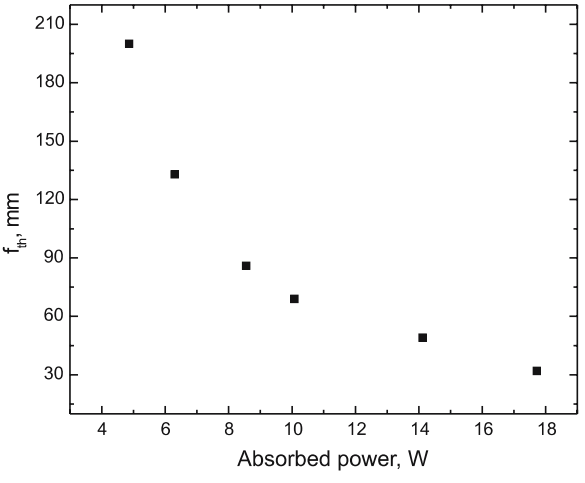

FIGURE 4 Thermal lens as a function of absorbed pump power

The astigmatic thermal lens makes the laser output mode elliptic and also causes different beam-quality parameter values along the axes of the ellipse. The M^2-values of the output beam were measured using a CCD-camera to capture the collimated laser beam as well as the beam after focusing by a 100-mm lens. The results are shown in Fig. 5. The output beam was TEM_{00} at low pump powers (< 4 W of absorbed power) but then M^2 rapidly increased with pump power. At an absorbed power of about 8 W it becomes evident that the beam quality is worse along the axis closest to N_m (solid squares in Fig. 5), in other words, along the thermal expansion axis X_1'.

As should be expected in a three-level system, the emission wavelength decreases significantly with increased output coupling. For low output coupling, i.e., low levels of population inversion, the maximum gain will be located in the long-wavelength regions with the lowest reabsorption losses, around 1050 nm, as evidenced in the cavity with $T = 1\%$ output coupling. As the population inversion is increased, the gain peak is shifted towards shorter wavelengths and increases in amplitude. Once the lasing threshold is reached, the gain remains clamped so the output wavelength should remain constant as the pump power is increased. It is largely the case in the investigated laser cavities except for a slight increase of the output wavelength (totally by 2–3 nm) with the pump power. It should be mentioned that this increase is small and comparable to the bandwidth of the free-running laser. We attribute this to the increased temperature in the crystal leading to higher thermal population of the sublevels in the lower laser level, which, in turn, increases the reabsorption losses at shorter wavelengths and shifts the maximum gain to longer wavelengths. The emission spectrum of the free-running laser was in most cases multi-peak with a bandwidth of about 3 nm. In order to reduce this bandwidth and tune the laser with an intracavity etalon, an output coupler with 100 mm radius of curvature had to be used to enable longer cavities. After inserting a 50 μm sapphire etalon, the emission became centered on a single peak with a bandwidth of ~ 150 pm. The

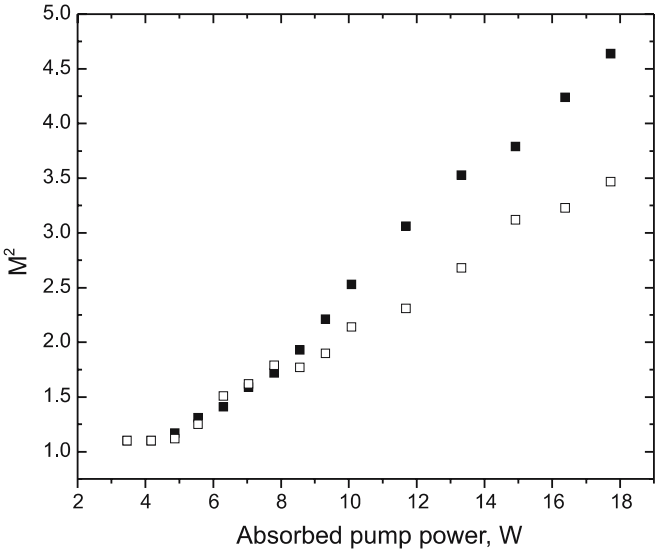

FIGURE 5 M^2-value along two principal directions in the elliptical cross section of the laser output beam. *Solid squares* – direction of the strongest thermal lens, *open squares* – perpendicular direction

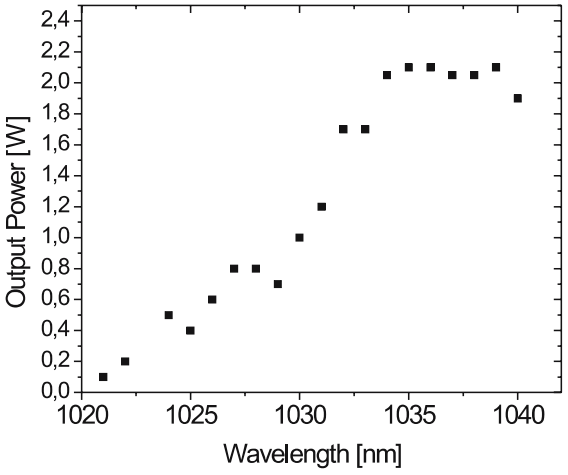

FIGURE 6 Output wavelength tuning using intracavity etalon

tuning of the emission wavelength was achieved by turning the etalon. Figure 6 shows an example of the tuning behavior obtained in a laser cavity with $T = 5\%$ output coupling and pumped at 12 W incident pump power. The output power was reduced by inserting the etalon, both because of insertion loss and because the cavity length had to be increased beyond the optimum value in order to make room for the etalon.

4 Conclusions

We have designed and optimized two different pump schemes for high power diode end-pumped Yb:KGW lasers. The pump scheme using a fiber delivery system gives an unpolarized but symmetric beam that exhibits high slope efficiency because of good overlap between the pump and the cavity mode. The pump scheme using focusing optics gives a polarized but asymmetric beam which exhibits substantially higher absorption which, combined with a mode overlap that is optimized by taking into account astigmatic thermal lens, leads to better optical efficiency. The optical-to-optical efficiency of 47% has been reached for both pumping configurations and we generated maximum 12.4 W of the output power. To our knowledge, this is the largest output power reported so far for single-pass end-pumped Yb:KGW lasers. The limit of the power scalability is reached due to thermal fracture of the laser crystal at an estimated temperature gradient of 1.2×10^5 K/m. Measurements of the thermal lens and M^2 parameter of the laser beam reveal substantial ellipticity developing at higher pump powers and related to the asymmetry of thermal expansion, thermal conductivity and thermooptic coefficients in the KGW laser host. Finally, due to the broad emission cross section bandwidth in Yb:KGW, the generated wavelength can be chosen between 1030 nm and 1050 nm in a free running laser cavity by simply choosing proper output coupling, although the maximum power has been achieved at wavelengths around 1040 nm. In this cavity, we demonstrated output wavelength tuning between 1021 nm and 1041 nm by using an intracavity etalon. Finally, we can speculate that with the fiber-coupled diode used in this work scaling up of the output power to at least 20 W seems feasible by (1) employing

an asymmetric (e.g., 3×1 mm) aperture of the laser crystal for more efficient cooling and (2) by using laser crystal with athermal cut for the beam propagation in the N_p–N_g plane, which would strongly reduce thermal lensing and astigmatism [20].

ACKNOWLEDGEMENTS The work has been supported in part by the EU project under contract NMP3-CT-2003-505580, Göran Gustafsson foundation, and by Saab Bofors Dynamics AB.

REFERENCES

1 A.A. Demidovich, A.N. Kuzmin, G.I. Ryabtsev, M.B. Danailov, W. Strek, A.N. Titov, J. Alloys Compd. **300–301**, 238 (2000)
2 K. Petermann, D. Fagundes-Peters, J. Johannsen, M. Mond, V. Peters, J.J. Romero, S. Kutovoi, J. Speiser, A. Giesen, J. Cryst. Growth **275**, 135 (2005)
3 M.C. Pujol, M.A. Bursukova, F. Güell, X. Mateos, R. Solé, Jna. Gavaldà, M. Aguiló, J. Massons, F. Díaz, P. Klopp, U. Griebner, V. Petrov, Phys. Rev. B **65**, 165 121 (2002)
4 N.V. Kuleshov, A.A. Lagatsky, A.V. Podlipensky, V.P. Mikhailov, G. Huber, Opt. Lett. **22**, 1317 (1997)
5 A.A. Lagatsky, N.V. Kulsehov, V.P. Mikhailov, Opt. Commun. **165**, 71 (1999)
6 S. Erhard, J. Gao, A. Giesen, K. Contag, A.A. Lagatsky, A. Abdolvand, N.V. Kuleshov, J. Aus der Au, G.J. Spühler, F. Brunner, R. Paschotta, U. Keller, Technical Digest. Summaries of papers presented at the Conference on Lasers and Electro-Optics 2001, 333-4
7 J. Liu, U. Griebner, V. Petrov, H. Zhang, J. Zhang, J. Wang, Opt. Lett. **30**, 2427 (2005)
8 P. Klopp, V. Petrov, U. Griebner, V. Nesterenko, V. Nikolov, M. Marinov, M.A. Bursukova, M. Galan, Opt. Lett. **28**, 322 (2003)
9 N.V. Kuleshov, A.A. Lagatsky, V.G. Shcherbitsky, V.P. Mikhailov, E. Heumann, T. Jensen, A. Diening, G. Huber, Appl. Phys. B **64**, 409 (1997)
10 F. Brunner, T. Sdmeyer, E. Innerhofer, F. Morier-Genoud, R. Paschotta, V.E. Kisel, V.G. Shcherbitsky, N.V. Kuleshov, J. Gao, K. Contag, A. Giesen, U. Keller, Opt. Lett. **27**, 1162 (2002)
11 A. Beyertt, D. Nickel, A. Giesen, Appl. Phys. B **80**, 655 (2005)
12 A. Brenier, G. Boulon, J. Alloys Compd. **323–324**, 210 (2001)
13 A. Brenier, J. Luminesc. **92**, 199 (2001)
14 L.D. DeLoach, S.A. Payne, L.L. Chase, L.K. Smith, W.L. Kway, W.F. Krupke, IEEE J. Quantum Electron. **29**, 1179 (1993)
15 M.C. Pujol, R. Solé, J. Massons, Jna. Gavaldà, X. Solans, C. Zaldo, F. Díaz, M. Aguiló, J. Appl. Cryst. **34**, 1 (2001)
16 S.A. Payne, L.L. Chase, H.W. Newkirk, L.K. Smith, W.F. Krupke, IEEE J. Quantum Electron. **24**, 2243 (1988)
17 V.E. Kisel, A.E. Troshin, V.G. Shcherbitsky, N.V. Kuleshov, in ASSP 2003 paper WB7
18 J.E. Hellström, S. Bjurshagen, V. Pasiskevicius, Appl. Phys. B **10** (2006), doi: 1007/s00340-005-2115-8
19 M.C. Pujol, X. Mateos, R. Solé, J. Massons, Jna. Gavaldà, X. Solans, F. Diaz, M. Aguiló, J. Appl. Cryst. **35**, 108 (2002)
20 S. Biswal, S. P. O'Connor, S.R. Bowman, Appl. Opt. **44**, 3093 (2005)